Chemical Geology 599 (2022) 120841

Contents lists available at ScienceDirect

Chemical Geology

journal homepage: www.elsevier.com/locate/chemgeo

Influence of precipitation rate and temperature on the partitioning of magnesium and strontium in calcite overgrowths

Mahmoud Alkhatib [a], Mutaz Qutob [a,*], Samia Alkhatib [a], Anton Eisenhauer [b]

[a] Al-Quds University, Jerusalem, Palestinian Authority, Israel
[b] GEOMAR Helmholtz-Zentrum für Ozeanforschung Kiel, 24148 Kiel, Wischhofstr. 1-3, Germany

ARTICLE INFO

Editor: Claudia Romano

Keywords:
Calcite
Aragonite
Precipitation rate
Magnesium
Strontium
Overgrowths

ABSTRACT

To study the incorporation of magnesium (Mg) and strontium (Sr) in calcite precipitated over synthetic calcite seeds (overgrowths) as a function of the precipitation rate (R*, μmol/m^2 h), we performed precipitation experiments wherein temperature and precipitation rates were decoupled at intervals of approximately 3.63–5.22 μmol/m^2 h. In most sample reactions, high-magnesium calcite (HMC) overgrowths co-precipitated with aragonite from the stirred solutions exposed to an atmosphere of NH_3 and CO_2 gases throughout the spontaneous decomposition of $(NH_4)_2CO_3$. The percentage of aragonite in the solid $CaCO_3$ increased with both temperature and dissolved inorganic carbon (DIC). The order of reaction with respect to the [DIC] is temperature dependent and is 1.9, 2.4, and 2.9 at temperatures of 12.5, 25.0, and 37.5 °C, respectively. The magnesium distribution coefficient (D_{Mg}) increases significantly with increasing R*, temperature, and Mg/Ca ratio in the fluid. The strontium distribution coefficient (D_{Sr}) increases with R* and with increasing $MgCO_3$ concentrations in the calcite overgrowths. However, it is independent of temperature.

1. Introduction

Calcium carbonate ($CaCO_3$) is one of the most abundant and reactive minerals in the natural environment, especially in marine sediments. Biogenic $CaCO_3$ comprises the majority of the mineral budget, while inorganic precipitates are minor contributors (Morse and Mackenzie, 1990). The solubilities of all pure carbonates decrease with increasing temperature in the following order: amorphous calcium carbonate (ACC) > vaterite > aragonite > calcite. Calcite is the most abundant, thermodynamically stable, and the least soluble polymorph of $CaCO_3$ (Plummer and Busenberg, 1982). In natural systems, calcite regularly includes Mg^{2+} in its lattice and may contain more than 20 mol% $MgCO_3$ (Folk, 1974; Morse, 1983; Morse et al., 1997; Davis et al., 2000). Calcite and Mg-bearing forms are typically classified into three groups. Calcite commonly refers to minerals containing less than 0.5 mol% $MgCO_3$ (Howson et al., 1987; Bar-Matthews et al., 1991). Low-magnesium calcite (LMC) contains up to 5 mol% $MgCO_3$, and high-magnesium calcite (HMC) contains more than 5.0 mol% $MgCO_3$ (Scoffin, 1987); however, this classification varies from author to author. Mg-calcite is more soluble than pure calcite, and as the content of Mg increases in the calcite, its solubility also increases (Morse and Mackenzie, 1990). The majority of sedimentary calcites are skeletal remains of coccolithophores and foraminifera, which are composed of LMC (>99% $CaCO_3$). Inorganic precipitated Mg-free calcite in the marine environment is not observed due to the inhibitory effect of Mg ions. Rather, $CaCO_3$ preferentially crystallizes as aragonite or magnesium calcite under normal condition (Folk, 1974). The presence of Mg ions in the aqueous solution inhibits calcite nucleation and reduces the calcite growth rate. This could be explained by two different models: the step pinning model (Kubota and Mullin, 1995; van Enckevort et al., 1996; De Yoreo and Vekilov, 2003; Astilleros et al., 2010) and the impurity incorporation model (Berner, 1975; Davis et al., 2000; De Yoreo and Vekilov, 2003). The step pinning model assumes that the adsorption of hydrated Mg^{2+} at the kink sites on step edges or at sites on the terraces causes the pinning of the steps, and as a result, the steps will advance at a slower rate. However, impurity adsorption is a reversible process, and an increase in supersaturation can cause the removal of the adsorbed impurities, causing the steps to grow again at the velocity corresponding to that of a pure solid at supersaturation. The impurity incorporation model assumes that Mg^{2+} is incorporated into the calcite structure, forming a solid solution. This structure is considered to be more soluble than the pure phase, resulting in an increase in the threshold supersaturation at

* Corresponding author.
E-mail address: kutob@staff.alquds.edu (M. Qutob).

https://doi.org/10.1016/j.chemgeo.2022.120841
Received 10 January 2022; Received in revised form 22 March 2022; Accepted 27 March 2022
Available online 31 March 2022

which crystallization begins.

Calcite and aragonite are $CaCO_3$ polymorphs that are most commonly found to coexist and coprecipitate in the same environment. Different physicochemical conditions control the formation of $CaCO_3$ polymorphs. Aragonite precipitation is favored by increasing both the temperature and Mg:Ca ratio of the fluid, while calcite is predominant at lower Mg:Ca ratios and temperatures (e.g., Morse and Mackenzie, 1990; Burton, 1993; Morse and He, 1993; Morse et al., 1997; Niedermayr et al., 2013). Reaction kinetics are crucial for polymorph selection (e.g., Given and Wilkinson, 1985; De Choudens-Sánchez and González, 2009); higher CO_3^{2-} accumulation rates, CO_3^{2-}/Ca^{2+} ratios, and dissolved inorganic carbonate (DIC) favor the formation of aragonite instead of calcite at certain Mg/Ca fluid ratios (Niedermayr et al., 2013). Another factor that significantly affects the nucleation and growth behavior of $CaCO_3$ polymorphs is the addition of organic compounds, such as polyaspartic acid, and inorganics, such as sulfate and orthophosphate ions (e.g., Bischoff, 1968; Mucci, 1986; Falini et al., 1994; Meldrum and Hyde, 2001; Niedermayr et al., 2013).

The enrichment of trace elements (as Mg and Sr) in biogenic and inorganic $CaCO_3$ relative to Ca reflects the specific environmental conditions (temperature, growth rate, pH, salinity, and the composition of seawater) at the time of formation (e.g., Morse and Bender, 1990; Lopez et al., 2009; Tang et al., 2012). In case of biogenic origins, the trace element contents are also affected by the species or biological effects (vital effects) (e.g., Urey et al., 1951; Weber and Woodhead, 1970; Weber and Woodhead, 1972; Elderfield et al., 1996; Lea et al., 1999). The trace elements to calcium ratios of biogenic and inorganic $CaCO_3$ provide a valuable proxy for oceanographic data, making them a beneficial tool for reconstructing the paleoenvironmental conditions of oceans. For example, Sr/Ca in calcite can be used as a proxy for the precipitation rate (e.g., Böhm et al., 2012; and AlKhatib and Eisenhauer, 2017a, 2017b, and Mg/Ca in calcite is considered to be a reliable proxy for the composition and temperature of paleo-seawater (e.g., Chave, 1954a, 1954b,; Rosenthal et al., 1997; Stanley and Hardie, 1998; Stanley, 1999; Elderfield and Ganssen, 2000; Dekens et al., 2002; Dickson, 2002; and Bryan and Marchitto, 2008).

Many experiments have been performed to clarify the factors affecting the incorporation of Mg in calcite. Temperature is one of the most significant factors. As the temperature increases, more Mg is incorporated in the calcite (e.g., Katz, 1973; Mucci, 1987). The second factor is the Mg/Ca fluid ratio; as this ratio increases in the precipitating solution, more Mg is incorporated in the calcite (e.g., Mucci and Morse, 1983; De Choudens-Sánchez and González, 2009). P_{CO2} may also affect the enrichment of Mg in calcite (e.g., Burton and Walter, 1991; Hartley and Mucci, 1996). Sulfate ions reduce the incorporation of Mg in calcite (e.g., Mucci et al., 1989; Zhong and Mucci, 1989). However, most previous studies have claimed that the precipitation rate has no effect on the amount of Mg present in the calcite. Lahann and Siebert (1982) suggested a strong influence of precipitation kinetics on the distribution of Mg^{+2} between the solution and crystals. However, Given and Wilkinson (1985) argued that there is a relationship between the crystal composition (enrichment of trace elements), morphology, mineralogy and the rate of precipitation. The crystal composition is apparently affected only by the solution Mg/Ca ratio. To determine the factors influencing the precipitation rate, we aimed to study the precipitation of Mg-calcite over pure calcite seeds (crystal overgrowths) as a function of precipitation rate at three different temperatures (12.5, 25, and 37.5 °C), while keeping the solution Mg/Ca ratio constant and using the same chemical setup as AlKhatib and Eisenhauer (2017a, 2017b).

2. Material and methods

2.1. Materials and experimental setup

Precipitation reactions were carried out using the same experimental setup described by AlKhatib and Eisenhauer (2017a, 2017b) to induce magnesium calcite overgrowths on calcite seeds from Mg-rich aqueous solutions, as illustrated in Fig. 1. The calcite seeds (Roth, $CaCO_3 > 99\%$, Art.-Nr.P012.2) had a surface area of 0.5 m^2/g, determined by both BET and SEM (AlKhatib and Eisenhauer, 2017b). The precipitation reactions were carried out on exactly 50.0 mg of seed material. All the chemicals were ACS grade Merck, and all the solutions were prepared using deionized water (18.2 MΩ). The solutions were prepared to precipitate $CaCO_3$ in ammonium buffered solutions (NH_4/NH_3) at three different temperatures: 12.5, 25.0, and 37.5 °C (±0.2 °C). The volume of the reaction solutions ranged between 330 and 400 mL. The solutions were composed of 0.395 M NH_4Cl and different concentrations of Ca^{2+} ions that range from 77 to 114 mM. In all experiments the molar ratio of Sr/Ca was constant and approximately 0.1. The molar ratio of Mg/Ca was also constant and approximately 2.9. An exception were in the reaction solutions, 1, 7, and 13; in these three solutions the Mg/Ca ratio was approximately 3.9, as indicated in Table 1.

In all the experiments, the reacting solution was stirred with a magnetic stirrer at 300 rpm. Ammonium carbonate decomposes spontaneously and produces an ammonia/carbon dioxide atmosphere within the chamber through the following reaction:

$$(NH_4)_2CO_3(S) \rightarrow 2NH_3(g) + CO_2(g) + H_2O(g) \quad (1)$$

Ammonia and carbon dioxide gases diffuse and dissolve in the experimental solution, increasing the pH and alkalinity through the following reactions:

$$NH_3(g) + H_2O \rightleftharpoons NH_4(aq) + OH^-(aq) \quad (2)$$

$$CO_2(g) + H_2O \rightleftharpoons CO_2(aq) \quad (3)$$

$$CO_2(aq) + H_2O \rightleftharpoons H_2CO_3 \quad (4)$$

$$H_2CO_3 \rightleftharpoons HCO_3^-(aq) + H^+(aq) \quad (5)$$

$$HCO_3^-(aq) \rightleftharpoons CO_3^{2-}(aq) + H^+(aq) \quad (6)$$

The overall spontaneous reaction of the steps (1)–(6) is:

$$(NH_4)_2CO_3(S) \rightleftharpoons 2NH_4^+(aq) + CO_3^{2-}(aq) \quad (7)$$

The result of these reactions is the supersaturation of the reacting solution with respect to calcite and aragonite. The dynamics of the reaction were monitored using a WTW 3100 pH meter, which was standardized using buffer solutions of pH 4, 7, and 10 before each experiment. This pH meter was connected to a computer that monitored the pH values and the temperature of the solution online continuously and stored the measured data in an Excel sheet. The pH of the reacting solution gradually increased until it reached a constant value and then decreased slightly, at which moment the precipitation of $CaCO_3$ started. The start of the precipitation was also characterized by a simultaneous decrease in the dissolved [Ca] in the solution at this pH. Throughout the reaction, the pH of the reacting solution (when precipitation starts) remained relatively constant (± 0.02 units), as well as its temperature during all the reactions (±0.2 °C). We controlled the rate of reaction as well as the time needed to reach the precipitation point using the quantity, the surface area of the ammonium carbonate granules, and porosity of the membrane through which the gases diffuse. For example, for slow reaction rates, we used 5–10 g of ammonium carbonate with a radius of approximately 1 cm. To accelerate the reactions, we placed an additional beaker containing solid ammonium carbonate (different quantities and different particle sizes) inside the reaction chamber. The beaker was covered with a parafilm of distinct porosity (certain number of holes were made by a pin). In certain cases, the beaker was not covered, and the rate of reaction increased rapidly.

During the experiment, the chemical evolution of the reacting solution was monitored by sampling 2 ml at distinct time intervals to be analyzed later. The intervals ranged between 2 and 30 min, depending on the reaction time. Each reaction was allowed to run for a certain

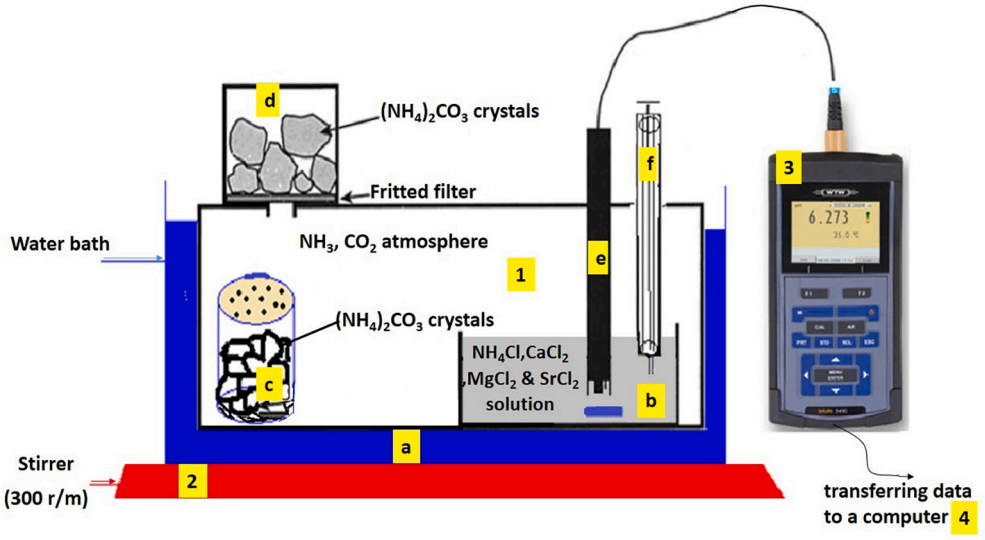

Fig. 1. schematic design of the experimental setup: (1) the reaction chamber which is a sealed plastic container consisting of a copper tubing (a) where water is circulating to keep a constant temperature, (b) beaker that contains the reacting solution, (c) a beaker that contains some ammonium carbonate granules that decompose spontaneously to provide ammonia and carbon dioxide gases, (d) fritted filter funnel that also contains some ammonium carbonate granules, (e) pH and temperature sensors, (f) syringe to withdraw samples from the reacting solution, (2) magnetic stirrer, (3) pH meter and (4) computer recording the measured data in an excel sheet.

period of time depending on its rate and then stopped by removing the reacting solution from the sealed chamber and filtering the solution as quickly as possible by vacuum filtration through a cellulose filter paper with a pore size of 0.2 μm. The solid was transferred to the filter paper, and then it was washed with deionized water (18.2 MΩ) that made slightly alkaline by mixing a small volume of pure ammonium hydroxide solution. The solid was finally washed with pure ethanol to remove any adsorbed $CaCl_2$, $MgCl_2$, or $SrCl_2$ aqueous solutions on the surface of the crystals; the solid was then dried in an oven overnight at 40 °C and weighed.

2.2. Analysis

2.2.1. Dissolved inorganic carbon (DIC)

The details used to determine the DIC in our system have been described earlier in AlKhatib and Eisenhauer (2017a). To calculate DIC, the total alkalinity (TA) of each experiment over the entire reaction period must be calculated. We did this by titrating 0.2 ml of the reaction mixture at different intervals of time during the precipitation reaction using 0.02 N HCl (dilution of MERCK-Titrisol-solution™). This HCl solution was initially standardized against IAPSO seawater (certified alkalinity of 2.325 mM) using a micro titration apparatus Metrohm 665 Dosimat equipped with a titration vessel of 7 cm. During the titration, the sample was continuously degassed with nitrogen to remove any CO_2. The indicator used in this titration was prepared from two solutions. Solution 1: approximately 32 mg Methyl Red (or 37 mg of sodium salt of Methyl Red) was mixed with 1.19 ml of 0.1 M NaOH and dissolved in 80 ml 96% ethanol. Solution 2: Approximately 10 mg of methylene blue was dissolved in 10 ml 96% ethanol. A greenish-brown solution was obtained by mixing 4.8 ml of Solution 2 with 80 ml of Solution 1, and at the end point of the titration, the solution became pink. In each titration, 20 μL of the indicator was added to 4.8 ml of water and 0.2 ml sample. Each sample was titrated three times, and the average volume of the titrant was used to calculate the total alkalinity. The concentrations of NH_3 and NH_4 in our experimental setup were relatively high, which inhibited the calculations of the activity coefficients of different species in the reacting aqueous solution by applying geochemical modeling and the PHREEQC software. Consequently, all the calculations were based only on the concentrations. The TA did not increase by more than 10% of the initial value at the precipitation point until the end of the reaction. Therefore, we determined the TA at the end of all the reactions (Table 1) and adopted this value for further calculations.

$$TA = [NH_3] + [HCO_3^-] + 2[CO_3^{2-}] \quad (8)$$

The $[NH_3]$ in our solutions was calculated following Lemarchand et al. (2004):

$$[NH3] = \frac{[Cl^-] + TA - 2[M^{2+}]}{\frac{[H^+]}{Ka} + 1} \quad (9)$$

where $[M^{2+}]$ is the concentration of metal divalent ions in the solution, $[Cl^-]$ is the concentration of chloride ions, $[H^+]$ is calculated from the pH values at the end of each experiment, and K_a is the apparent ammonium acid dissociation constant. The K_a values at different temperatures were calculated using Eq. (10), which was derived by AlKhatib and Eisenhauer (2017a).

$$pKa = 2651.4/T + 0.60 \quad (10)$$

where T is the temperature in Kelvin. The values of $[NH_3]$ are listed in Table 1. The DIC is equal to the difference between the TA and $[NH_3]$, as shown in Table 1. The $[CO_3^{2-}]$ in our solutions was calculated (Table 1) following Lemarchand et al. (2004): (Eq. (11)).

$$[CO_32^-] = \frac{TA - [NH_3]}{\frac{[H^+]}{K2} + 2} \quad (11)$$

where K_2 is the second dissociation constant of carbonic acid; it was equal to 4.9×10^{-10}, 8.5×10^{-10}, and 1.5×10^{-9} at temperatures of 12.5, 25, and 37.5 °C, respectively. These were calculated following Millero (1995): (Eq. (12)).

$$ln K_2 = -0.84 - 3741.13/T - 1.44 ln(T) + (-0.13 - 24.41/T) S^{0.5} + 0.12S - 0.01S^{1.5} \quad (12)$$

where T is the temperature in Kelvin, and S is the average salinity (75) of the solutions.

The saturation state (Ω) with respect to calcite and aragonite was calculated according to Millero (1995): (Eq. (13)).

$$\Omega = [Ca^{2+}][CO_3^{2-}]/K_{sp} \quad (13)$$

where the solubility product constants (K_{sp}) of calcite and aragonite at a salinity of 75 were calculated as a function of the temperature, as in Millero (1995). The values of K_{sp} are listed in Table 2. The saturation index (SI) with respect to calcite and aragonite = log Ω is included in Table 1.

Table. 1

Volume of solution, temperature (T), pH, total alkalinity (TA), concentration of ammonia, dissolved inorganic carbon (DIC), carbonate and bicarbonate ions concentrations, time of precipitation reaction, initial and final concentrations of Ca, fraction of calcium remaining in aqueous solution after precipitation, Mg/Ca and Sr/Ca ratios in the initial solution, saturation index for calcite and aragonite (SI), mass of $CaCO_3$ precipitated, percentage of aragonite in the bulk solid (calcite seeds + product), mass of aragonite in the product, mass of calcite in the product, percentage of aragonite and calcite in $CaCO_3$ precipitate, and surface area of calcite and aragonite precipitate.

Sample label	Volume of \vskip5 \hfill \hbox \rot90 {solution/ ml	T/ °C ± 0.2	pH	TA \vskip5 \hfill \hbox \rot90 {/mM	$[NH_3]$/ mM	DIC/ mM	$[CO_3]$ mM	$[HCO_3]$ mM	Time of \vskip5\hfill \hbox\rot90 {Precipitation/ h	$[Ca]_0$/mM ± 2σ	$[Ca]_f$ /mM ± 2σ	Fraction of Ca \vskip5 \hfill \hbox \rot90 {remain	$[Mg]/[Ca]_0$ \vskip5 \hfill \hbox \rot90 {Molar ratio	$[Sr]/[Ca]_0$ \vskip5 \hfill \hbox \rot90 {Molar ratio	SI. calcite	SI. aragonite	Mass of \vskip5 \hfill \hbox \rot90 {CaCO3/ mg	% aragonite in \vskip5 \hfill \hbox \rot90{ Bulk solid	Mass \vskip5 \hfill\hbox \rot90 {aragonite/ g	Mass \vskip5 \hfill \hbox \rot90 {Calcite/ g	% aragonite in \vskip5 \hfill \hbox \rot90 {$CaCO_3$	% calcite in \vskip5 \hfill \hbox \rot90 {$CaCO_3$	Area of calcite \vskip5 \hfill \hbox \rot90 {/m^2	Area of \vskip5 \hfill \hbox \rot90{ Aragonite/ m^2
1	2	3	4	5	6	7	8	9	10	11	12	13	14	15	16	17	18	19	20	21	22	23	24	25
1	330	12.5	7.536	10.00	4.43	5.57	0.09	5.39	4.68	79.14 ± 0.01	78.55 ± 0.02	0.993	3.86	0.13	0.62	0.38	19	n.d	n.d	0.019	n.d	100	0.010	n.d
2	370	12.5	7.332	9.00	2.77	6.23	0.06	6.10	1.53	98.35 ± 0.01	97.43 ± 0.02	0.991	2.96	0.11	0.54	0.30	34	n.d	n.d	0.034	n.d	100	0.017	n.d
3	370	12.5	7.573	10.88	4.83	6.05	0.11	5.84	2.47	95.81 ± 0.01	94.67 ± 0.01	0.988	3.03	0.11	0.79	0.55	42	n.d	n.d	0.042	n.d	100	0.021	n.d
4	400	12.5	7.449	11.52	3.64	7.88	0.11	7.67	0.93	110.77 ± 0.01	110.05 ± 0.01	0.994	2.84	0.10	0.86	0.61	29	10	0.008	0.021	27	73	0.011	0.021
5	400	12.5	7.610	15.22	5.31	9.91	0.19	9.53	1.27	113.22 ± 0.03	111.47 ± 0.04	0.985	2.84	0.10	1.10	0.86	70	25	0.030	0.040	43	57	0.020	0.081
6	400	12.5	7.475	10.75	3.86	6.89	0.10	6.69	4.40	114.05 ± 0.01	110.73 ± 0.01	0.971	2.84	0.10	0.83	0.59	132	20	0.037	0.095	28	72	0.048	0.100
7	330	25	8.015	19.60	13.35	6.25	0.45	5.34	0.50	76.83 ± 0.05	73.95 ± 0.04	0.963	3.90	0.13	1.33	1.07	95	34	0.050	0.045	53	47	0.022	0.136
8	400	25	8.148	23.00	18.08	4.92	0.46	4.00	0.94	104.64 ± 0.02	103.62 ± 0.01	0.990	2.96	0.10	1.47	1.21	41	20	0.018	0.023	44	56	0.011	0.049
9	400	25	7.732	18.76	7.07	11.69	0.48	10.74	0.47	105.20 ± 0.01	101.45 ± 0.01	0.964	2.96	0.10	1.49	1.22	150	50	0.100	0.050	67	33	0.025	0.271
10	400	25	8.185	29.84	19.93	9.91	0.99	7.92	0.70	102.35 ± 0.01	97.45 ± 0.01	0.952	2.96	0.10	1.80	1.53	196	50	0.125	0.071	64	36	0.035	0.339
11	400	25	8.284	34.56	25.01	9.55	1.14	7.26	0.67	103.24 ± 0.01	98.62 ± 0.01	0.955	2.91	0.10	1.86	1.60	185	50	0.117	0.068	63	37	0.034	0.315
12	400	25	8.236	34.88	22.55	12.33	1.36	9.62	0.93	112.88 ± 0.05	103.43 ± 0.05	0.916	2.91	0.10	1.98	1.71	378	70	0.299	0.079	79	21	0.040	0.806
13	330	37.5	8.090	23.44	15.92	7.52	0.92	5.68	0.96	79.03 ± 0.02	76.91 ± 0.01	0.973	3.80	0.13	1.67	1.40	70	45	0.054	0.016	77	23	0.008	0.146
14	400	37.5	8.255	36.32	23.58	12.74	2.05	8.64	0.34	104.39 ± 0.01	101.24 ± 0.03	0.970	2.91	0.10	2.14	1.87	126	65	0.115	0.011	91	9	0.006	0.310
15	400	37.5	7.864	15.43	9.43	6.00	0.49	5.03	2.00	101.45 ± 0.01	99.57 ± 0.05	0.981	2.91	0.10	1.51	1.23	75	40	0.050	0.025	67	33	0.012	0.136
16	400	37.5	8.100	28.00	11.54	12.34	2.05	8.23	0.12	104.44 ± 0.01	103.47 ± 0.01	0.991	2.91	0.10	2.14	1.87	39	40	0.035	0.004	91	9	0.002	0.096
17	400	37.5	8.332	42.40	28.25	14.15	2.56	9.03	0.65	102.03 ± 0.04	95.78 ± 0.05	0.939	2.91	0.10	2.23	1.95	250	80	0.240	0.010	96	4	0.005	0.648
18	400	37.5	8.060	23.28	14.89	8.39	0.98	6.44	1.13	106.20 ± 0.05	103.25 ± 0.04	0.972	2.91	0.10	1.83	1.55	118	60	0.100	0.018	85	15	0.009	0.271

Notes: n.d. (not detected), TA was measured by titrating the final solution with HCl, and the pH was measured at the end of each reaction. $[NH_3]$, $[CO_3^{2-}]$, and $[HCO_3^-]$ were calculated using Eqs. (9), (11), and (8), respectively, [DIC] = TA- $[NH_3]$, SI = log Ω, Ω calculated using Eq. (13), mass of $CaCO_3$ was calculated using Eq. (14) and is also equal to the mass of the bulk solid at the end of each experiment – 50 mg (50 mg = mass of added calcite seeds at the beginning of each experiment), percentage of aragonite in the bulk solid measured directly using XRD, mass of aragonite = % aragonite in bulk solid × mass of the bulk solid (mass of bulk solid = mass of $CaCO_3$ produced +50 mg), mass of calcite overgrowths (column 21) = column 18 − column 20, areas of calcite and aragonite are equal to mass of each mineral × its specific surface area (specific surface areas are 0.5 m^2/g and 2.7 m^2/g for calcite and aragonite, respectively).

Table 2
Solubility product constant (K_{sp}) of calcite and aragonite at a salinity 75 are calculated as function of temperature as in Millero (1995).

Solid	Ksp at 12.5 °C × 10^6	Ksp at 25 °C × 10^6	Ksp at 37.5 °C × 10^6
Calcite	1.69	1.62	1.54
Aragonite	2.96	2.93	2.91

2.2.2. Elemental analysis

The concentrations of Ca, Mg, and Sr ions in the solutions at different time intervals during each reaction were measured, as reported in Table 1. Furthermore, after the dissolution of the bulk solid carbonate sample consisting of the CaCO3 precipitate and 50 mg of pure calcite seed crystals, the elemental ratio was measured using inductively coupled plasma mass spectrometry (ICP-MS, Agilent 7500cx) with indium (In) as the internal standard. All the samples were diluted in 2% HNO_3 to reach 25.0 ± 2.5 ppm [Ca^{2+}] to avoid matrix effects. In the final solutions, [Mg^{2+}] was exceptionally close to that in the initial solutions, and the decrease in concentration was within the uncertainty of the initial concentration. For quality control and accuracy, indium (In) was used as the internal standard in combination with a multi-standard calibration method (Ca, Mg, and Sr in 2% HNO_3-ultra pure distilled HNO_3). Each sample was analyzed at least three times. For analyzing the solid products, the solid was mixed well to ensure a homogeneous composition after being filtered, washed, and dried. Then small samples were taken and diluted in 2% HNO_3 until the mixture contained approximately 25.0 ± 2.5 ppm Ca in order to avoid matrix effects, and then the metal ions were measured using the same method as that for other liquid solutions. Taking into account that exactly 50.0 mg of the bulk solid consisted of pure calcite seeds, the mass of $CaCO_3$ produced was 50 mg less than the mass of the bulk solid at the end of each experiment. The molar ratios of Mg/Ca and Sr/Ca in the solid product of $CaCO_3$ (equal to the ratios in the bulk solid multiplied by the ratio [mass bulk solid/mass of $CaCO_3$]) were calculated and are reported in Table 3, Columns 7 and 8, respectively. Coral standard JCP-1 was used as a reference material and measured for every fifth sample for a total of 10 times during this study ($N = 10$). The JCP-1 Sr/Ca and Mg/Ca ratios were calculated to be 8.82 ± 0.03 and 4.22 ± 0.04 mmol/mol respectively, which are consistent with the reported values of 8.84 ± 0.09 Sr/Ca and 4.2 ± 0.1 Mg/Ca mmol/mol Hathorne Ed et al. (2013) within statistical uncertainty.

2.2.3. Mineralogy of the precipitates

The samples were analyzed using an X-ray diffractometer (D8 Discover, Bruker AXS) in the 2Θ-range from 4° to 90°, with a step size of 0.007° and counting time of 1.5 s/step using a Cu X-ray radiation source (three arbitrarily selected XRD spectra and their important data peaks are shown in the Appendix A). The software was evaluated using High Score Plus Version 3.0d (3.0.4) by PANalytical. All measurements were performed at the Department of Geology, Kiel University.

The mass of the $CaCO_3$ product (Table 1, Column 18) was calculated by subtracting the mass of the calcite seeds (50.0 mg), which were initially added to the reacting solutions to induce calcite precipitation overgrowth, from the mass of the bulk solid, which was quantitatively filtered and dried at the end of each sample precipitation experiment. The mass of the $CaCO_3$ product agrees with the difference between $[Ca]_o$ and $[Ca]_f$ (Table 1, Columns 11 and 12, respectively). Theoretically, the mass of the $CaCO_3$ product can be calculated using Eq. (14).

$$CaCO_3\ \text{mass (mg)} = \frac{[Ca]o - [Ca]f}{1000} \times \frac{V(ml)}{1000} \text{x Fwt } CaCO_3 \times 1000 \qquad (14)$$

where *Fwt* is the molar mass = 100 g/mol.

The X-ray-D measurements indicated that all the bulk solid samples were either pure calcite or mixtures of calcite and aragonite, without detecting any other carbonates. The percentage of aragonite in the bulk solid samples is listed in Table 1, Column 19. The mass of aragonite in any sample product equals the percentage of the aragonite in the bulk solid multiplied by the mass of the bulk solid (mass of $CaCO_3$ product +50.0 mg)(Table 1 Column 20). The mass of calcite in the product equals the mass of the $CaCO_3$ product minus the mass of aragonite, as reported in Table 1, Column 21.

3. Results

3.1. Precipitation rate (R) and crystalline structure of $CaCO_3$ product

Knowing the values of the pH, [TA], [NH_3], and [DIC] is necessary to interpret the results of the precipitation rate (R) (mM/h) and the crystalline structure of the $CaCO_3$ product. The details of these quantities, as well as the metal ion concentrations in the initial and final solutions, are summarized in Table 1. The reacting solutions at all temperatures were supersaturated with calcite and aragonite (Table 1). The remaining fraction of Ca^{2+} at the end of all the precipitation reactions was more than 91% (Table 1). So we could apply the initial rate method to solve the rate of $CaCO_3$ precipitation. As an example of all the reactions, we plotted [Ca^{2+}] versus time for the randomly selected Sample 7 at 25 °C and fitted the curve to a linear equation (Fig. 2). The rate of precipitation (R) is equal to the slope (5.8 mM/h) of the straight line. For all reactions, less than 9% of Ca was consumed through precipitation, and the initial rate equaled the average rate, which was equal to the difference between the initial and final [Ca^{2+}] divided by the time of the precipitation reaction. For example, the average rate in Sample Reaction 7 = ((76.83 ± 0.05) – (73.95 ± 0.04))/0.5 = 5.76 ± 0.13 mM/h. The initial rate (mM/h) of $CaCO_3$ precipitation is listed in Table 3. For all temperatures, a direct relationship between *R* and *DIC* can be seen in Fig. 3. When plotting log*R* against *log[DIC]*, Samples 1, 7, and 13 were excluded because [Ca^{2+}] was approximately 80 mM in those samples, which differed from the concentration in other plotted samples (approximately 100 mM), and their Mg/Ca fluid ratio (≈3.9) was higher than that of the other plotted samples (≈2.9). The slopes of the curves in Fig. 3 are equal to the order of reaction with respect to the [DIC]. They increase slightly as a function of temperature, with values of 1.8, 2.4, and 2.8 at temperatures of 12.5, 25, and 37.5 °C, respectively, following the same pattern as the order of reaction as function of temperature for calcite overgrowths, as reported by Burton and Walter (1987).

From the XRD analysis (Table 1) only three sample reactions produced a homogeneous product (calcite overgrowths), which were at 12.5 °C when the DIC was less than or equal 6.23 mM. The remaining sample products were heterogeneous (a mixture of high-magnesium calcite (HMC) overgrowths and aragonite). The mineralogy of the $CaCO_3$ produced in this study was governed by the DIC and temperature, as demonstrated in Fig. 4 and Table 1. As the temperature and DIC increased, the percentage of aragonite in the $CaCO_3$ increased which is consistent with previous studies (e.g., Niedermayr et al., 2013).

To investigate whether the composition of the calcite overgrowths is dependent on the reaction rate, it was necessary to estimate the amount of Mg and Sr incorporated in the calcite overgrowths. To do this, we assumed that the specific surface area of the produced calcite overgrowths was equal to that of the calcite seeds = 0.5 m^2/g. We also assumed that the aragonite produced in this work was identical to that produced by AlKhatib and Eisenhauer (2017b), with the same specific surface area (2.7 m^2/g) and the same composition as a function of temperature and precipitation rate, because both studies used the same apparatus under the same conditions. Finally, we assumed that both minerals (aragonite and magnesium calcite overgrowths) precipitated simultaneously during the same period of the reaction. The area of the mineral was calculated as the specific surface area of the mineral multiplied by its mass. The surface areas of the produced calcite and aragonite solids are reported in Table 1, Columns 24 and 25, respectively. The normalized rates of precipitation R^* (μmol/m^2·h) of calcite and aragonite are summarized in Table 3, Columns 3 and 5, respectively, and were calculated using Eq. (15).

Table 3
Initial rate (R), normalized rate to the surface area (R*), molar % of $MgCO_3$ and %$SrCO_3$ in $CaCO_3$, calculated D_{Mg} and D_{Sr} in aragonite and in calcite overgrowths, and calculated percentage of $MgCO_3$ and %$SrCO_3$ in aragonite and in calcite products.

Sample label	Rate (R)/ (mM/ h)	Normalized rate of calcite (R*)/ μmol/m^2·h	Log R* calcite	Normalized rate of aragonite (R*)/μmol/ m^2·h	Log R* aragonite	Molar % $MgCO_3$ in $CaCO_3$ ± 2σ	Molar % $SrCO_3$ in $CaCO_3$ ± 2σ	Calculated \vskip5 \hfill \hbox \rot90{ log D_{Mg}-aragonite	Calculated \vskip5 \hfill \hbox \rot90 {D_{Mg}-aragonite	Calculated Mg/Ca molar ratio in aragonite	Calculated % Mg/Ca molar ratio in calcite	D_{Mg} in calcite	Log D_{Mg} in calcite	±(2SEM)	Calculated \vskip5 \hfill \hbox \rot90{log D_{Sr}-aragonite	Calculated \vskip5 \hfill \hbox \rot90 {D_{Sr}-aragonite	Calculated Sr/Ca molar ratio in aragonite	Calculated % Sr/Ca molar ratio in calcite	DSr-Calcite	Log DSr-Calcite	±2σ
1	2	3	4	5	6	7	8	9	10	11	12	13	14	15	16	17	18	19	20	21	22
1	0.12	4274	3.63			4.9 ± 0.04	2.5 ± 0.04				4.92	0.013	−1.90	0.024				2.46	0.190	−0.722	0.024
2	0.60	13,072	4.12			6.5 ± 0.04	3.6 ± 0.03				6.50	0.022	−1.66	0.016				3.60	0.338	−0.471	0.015
3	0.48	8097	3.91			5.0 ± 0.04	3.1 ± 0.03				5.00	0.016	−1.79	0.008				3.14	0.295	−0.531	0.009
4	0.77	21,505	4.33	3982	3.60	6.1 ± 0.03	6.4 ± 0.03	−2.66	2.20E-03	0.0063	8.07	0.028	−1.55	0.012	0.064	1.16	0.120	4.34	0.420	−0.377	0.012
5	1.38	15,748	4.20	2916	3.46	4.9 ± 0.04	8.1 ± 0.06	−2.75	3.84E-03	0.0110	7.82	0.027	−1.56	0.018	0.068	1.17	0.120	5.17	0.501	−0.300	0.018
6	0.75	4545	3.66	842	2.93	2.4 ± 0.01	4.6 ± 0.02	−3.10	6.87E-04	0.0020	3.30	0.011	−1.94	0.003	0.083	1.22	0.125	1.46	0.140	−0.854	0.007
7	5.80	40,000	4.60	7407	3.87	8.5 ± 0.04	10.3 ± 0.05	−2.88	1.30E-03	0.0052	17.50	0.044	−1.36	0.014	0.073	1.18	0.153	4.72	0.360	−0.444	0.014
8	1.10	21,277	4.33	3940	3.60	4.8 ± 0.05	6.7 ± 0.08	−2.99	1.03E-03	0.0031	8.33	0.028	−1.55	0.017	0.062	1.15	0.115	2.86	0.285	−0.544	0.021
9	8.00	42,553	4.63	7880	3.90	5.4 ± 0.06	10.2 ± 0.09	−2.87	1.33E-03	0.0040	15.55	0.052	−1.29	0.003	0.075	1.19	0.118	6.94	0.690	−0.161	0.006
10	7.00	28,571	4.46	5291	3.72	4.4 ± 0.05	9.4 ± 0.07	−2.94	1.15E-03	0.0035	11.60	0.038	−1.42	0.003	0.068	1.17	0.116	5.37	0.531	−0.275	0.006
11	6.90	29,851	4.47	5528	3.74	5.5 ± 0.05	10.3 ± 0.13	−2.93	1.17E-03	0.0035	14.27	0.048	−1.32	0.002	0.068	1.17	0.120	7.30	0.702	−0.154	0.008
12	10.10	21,505	4.33	3982	3.60	2.6 ± 0.02	9.9 ± 0.03	−2.99	1.03E-03	0.0031	11.20	0.037	−1.43	0.005	0.062	1.15	0.119	2.60	0.243	−0.614	0.007
13	2.20	20,833	4.32	3858	3.59	6.5 ± 0.06	12.0 ± 0.13	−3.14	7.23E-04	0.0028	27.33	0.071	−1.15	0.007	0.011	1.03	0.132	8.02	0.620	−0.207	0.010
14	9.30	58,824	4.77	10,893	4.04	2.9 ± 0.01	10.8 ± 0.05	−3.07	8.57E-04	0.0025	29.22	0.099	−1.00	0.008	0.025	1.06	0.109	9.84	0.952	−0.021	0.007
15	0.90	10,000	4.00	1852	3.27	3.4 ± 0.01	9.8 ± 0.04	−3.19	6.40E-04	0.0019	9.92	0.034	−1.47	0.017	0.001	1.00	0.103	8.72	0.843	−0.074	0.017
16	8.00	166,667	5.22	30,864	4.49	4.1 ± 0.03	13.1 ± 0.11	−2.99	1.02E-03	0.0030	42.55	0.146	−0.84	0.009	0.040	1.10	0.113	31.35	3.064	0.486	0.009
17	9.60	30,769	4.49	5698	3.76	1.8 ± 0.01	10.7 ± 0.09	−3.11	7.71E-04	0.0023	39.45	0.132	−0.88	0.006	0.016	1.04	0.107	10.38	1.005	0.002	0.008
18	2.60	17,699	4.25	3278	3.52	2.1 ± 0.02	11.7 ± 0.03	−3.15	7.03E-04	0.0021	12.98	0.044	−1.36	0.013	0.008	1.02	0.105	11.37	1.102	0.042	0.013

Notes: For all reactions, the initial rate (mM/h) equals the average rate as shown in the text for sample reaction 7, R* for both calcite and aragonite are calculated using Eq. (15) in the text, molar %$MgCO_3$, and % $SrCO_3$ in $CaCO_3$ products are calculated from the ratios in the bulk solids time ratio (mass of bulk solid/mass of $CaCO_3$ product), logD_{Mg} values in aragonite were estimated from the previous study of AlKhatib and Eisenhauer, 2017b, using Eqs. (16), (17), and (18) for temperatures 12.5, 25, and 37.5 °C respectively, logD_{Sr} values in aragonite were estimated from the previous study of AlKhatib and Eisenhauer, 2017b, using Eqs. (19), (20), and (21) for temperatures 12.5, 25, and 37.5 °C respectively, Mg/Ca and Sr/Ca molar ratios in aragonite (columns 11 and 18) were calculated using Eq. (22), Mg/Ca and Sr/Ca molar ratios in calcite (columns 12 and 19) using Eq. (23) in the text.

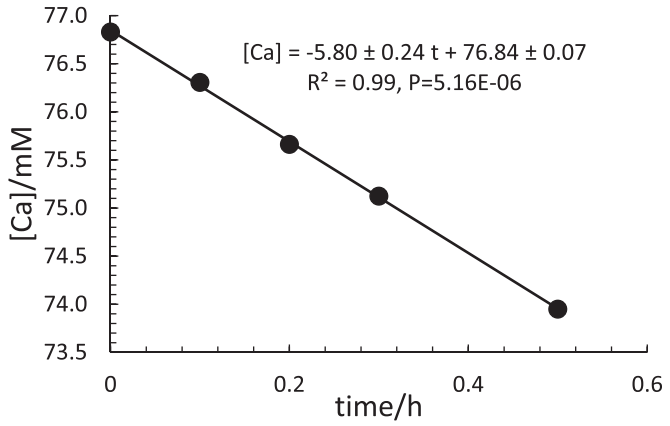

Fig. 2. Changes of Ca^{2+}-ion concentration as function of time for arbitrarily selected sample reaction 7 at 12.5 °C. Slope of the straight line equals the rate of reaction (R).

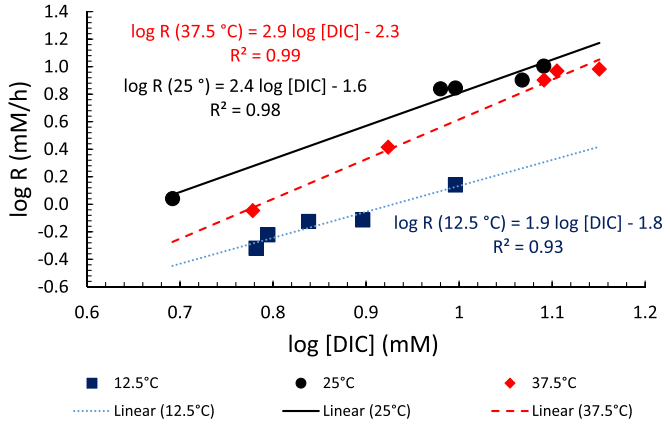

Fig. 3. log R (mM/h) versus log DIC (mM) at different temperatures for all samples (except samples 1,7and 13 which have large Mg/Ca ratio in the aqueous soluitio). The slopes of these lines equal the orders of reaction with respect to dissolved inorganic carbon (DIC). The order of reaction increases with temperature.

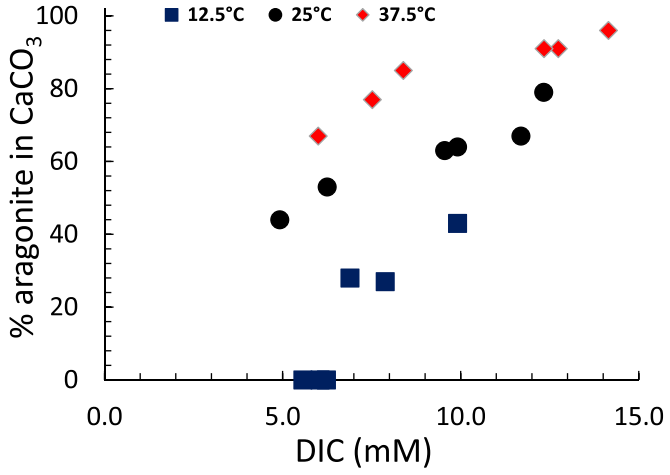

Fig. 4. The relation between % aragonite in the solid product mixture and dissolved inorganic carbon [DIC] as function of temperature. It increases with increasing DIC and temperature.

$$R^* = \frac{\mu\text{mol of mineral produced}}{\text{area of mineral produced } (m^2) \times \text{time of reaction (h)}} \quad (15)$$

where the *μmol* of each mineral = [*mass* (gm)/*Fwt* (g/mol)] × 10^6.

3.2. Incorporation of Mg and Sr in calcite growing overgrowths

The enrichment of Mg in argonite was calculated from AlKhatib and Eisenhauer (2017b) depending on similar conditions of the most important two variables which are precipitation rate and temperature and not on the value of pH at the end of the precipitation. The important factor is the total dissolved carbon which govern the precipitation rate and not the pH, The Mg in Calcite was not estimated in the same way because calcite was not precipitated in the presences of any Mg Ion, AlKhatib and Eisenhauer (2017a). If the precipitation of calcite in the previous work of AlKhatib and Eisenhauer (2017a) was not seeded with calcite the precipitate will be only aragonite as shown in AlKhatib and Eisenhauer (2017b).

To estimate the metal ions (Mg and Sr) incorporated in the magnesium calcite, described as the distribution of the metal in the aqueous solution and $CaCO_3$ (D_M), we first estimated the metal ions incorporated in the aragonite. We assumed that the metal distribution constants in the aragonite produced in this work were equal to those at the same R^* and temperature from AlKhatib and Eisenhauer (2017b). Figs. 5 and 6 summarize the values of $logD_{Mg}$ and $logD_{Sr}$ for aragonite, respectively, as a function of R^* and temperature from the AlKhatib and Eisenhauer (2017b). The $logD_{Mg}$ and $logD_{Sr}$ of the aragonite precipitated in this work could be estimated using Eq. (16) to Eq. (21), which were derived from Fig. 5 and Fig. 6.

$$\text{At } 12.5^\circ C,\ logD_{Mg} = 0.66\ logR^* - 5.04 \quad (16)$$

$$\text{At } 25^\circ C,\ logD_{Mg} = 0.38\ logR^* - 4.34 \quad (17)$$

$$\text{At } 37.5^\circ C,\ logD_{Mg} = 0.16\ logR^* - 3.73 \quad (18)$$

$$\text{At } 12.5^\circ C,\ logD_{Sr} = -0.029\ logR^* + 0.168 \quad (19)$$

$$\text{At } 25^\circ C,\ logD_{Sr} = 0.041\ logR^* - 0.084 \quad (20)$$

$$\text{At } 37.5^\circ C\ logD_{Sr} = 0.032\ logR^* - 0.104 \quad (21)$$

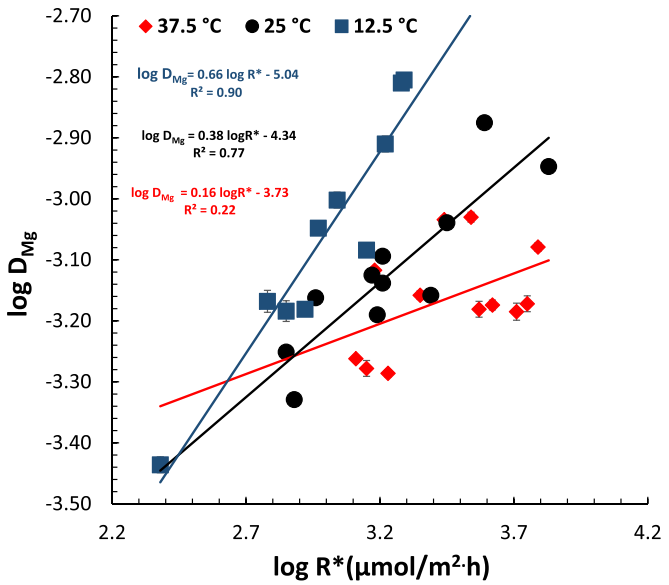

Fig. 5. Results of AlKhatib and Eisenhauer (2017b); log D_{Mg} in aragonite as function of log R* (μmol/m^2·h) at different temperatures.

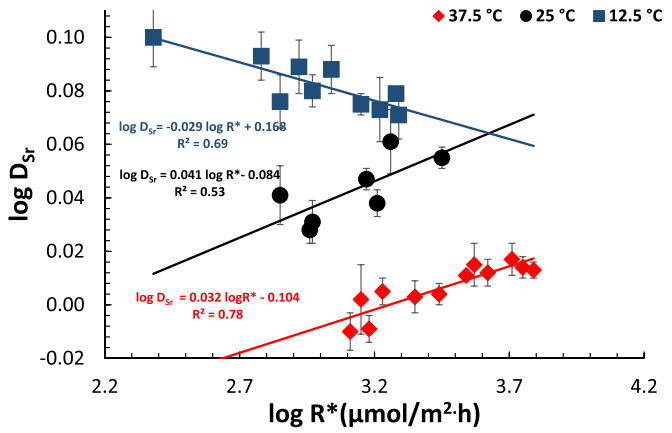

Fig. 6. Results of AlKhatib and Eisenhauer (2017b); log D_{Sr} in aragonite as function of log R* (µmol/m^2·h) at different temperatures.

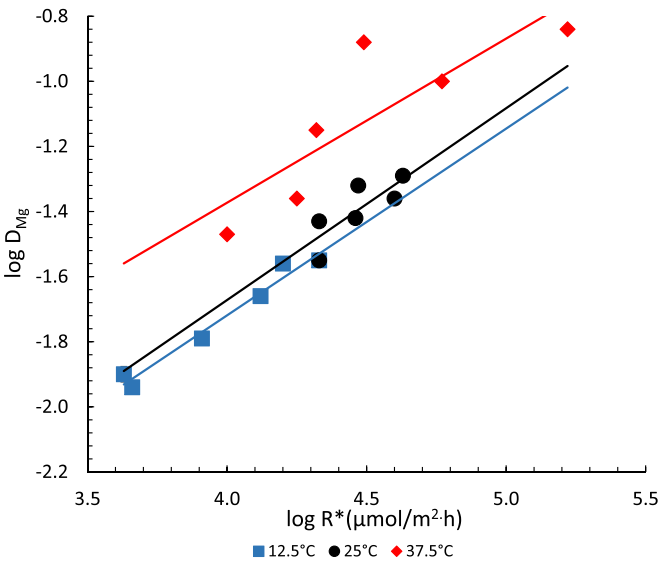

Fig. 7. log D_{Mg} in magnesium calcite overgrowths at different temperatures versus log R* (µ.mol/m^2 h). The log D_{Mg} values increase with increasing R* and with increasing temperature, clearly indicating that there is a separate effect of temperature and R*.

The estimated $logD_{Mg}$ and $logD_{Sr}$ values of the aragonite precipitated in this work are reported in Table 3, Columns 9 and 16, respectively.

The M/Ca molar ratios in $CaCO_3$ were calculated using Eq. (22), as described by Usdowski (1975).

$$([M]/[Ca])_{CaCO3} = ([M]/[Ca])_{aq,0} \times \left\{\left\{1-([Ca]/[Ca]_0)^{DM}_{aq}\right\}\Big/\left\{1-([Ca]/[Ca]_0)_{aq}\right\}\right. \quad (22)$$

where $([M]/[Ca])_{CaCO3}$ is the molar ratio of $CaCO_3$; $([M]/[Ca])_{aq,0}$ is the molar ratio of these ions in the initial solution; and $([Ca]/[Ca]_0)$ is the fraction of calcium that remains in the aqueous solution. The Mg/Ca and Sr/Ca molar ratios in the aragonite are reported in Columns 11 and 18, respectively, of Table 3. The metal/Ca molar ratio in the calcite was calculated using Eq. (23).

4. Discussion

To achieve the goal of this study, which is to determine the effect of growth rate of Mg incorporation in calcite overgrowths, most sample reaction fluids, except for samples 1, 7, and 13 (ratio of approximately 3.9), were prepared with an almost constant Mg/Ca ratio (approximately 2.9), as demonstrated in Table 1, Column 14. They were used to compare the extent of magnesium enrichment in calcite as a function of

$$M/Ca-_{calcite} = \left([M/Ca_{CaCO3\ mixture}]-[M/Ca-_{aragonite} \times \text{aragonite ratio} - _{CaCO3}]\right)/\text{calcite ratio} - _{CaCO3} \quad (23)$$

The calculated Mg/Ca molar ratio and Sr/Ca molar ratio in the calcite are listed in Table 3, Columns 12 and 19, respectively. The distribution constants of Mg and Sr in the aqueous solution and calcite were calculated using Eq. (22) in Table 3, Columns 13 and 20, respectively.

From Fig. 7, we see that for all temperatures, as the precipitation rate (R^*) increases, more magnesium is incorporated in the calcite (D_{Mg} increases). At a constant R^*, as the temperature increases, more Mg is incorporated in the calcite. The calcite produced can be classified as high-magnesium calcite (HMC) because for all sample reactions (except for sample reactions 1 and 6), the mol% of $MgCO_3$ in the calcite overgrowths is more than 5% (Table 3, Column 12).

As shown in Fig. 8, as the precipitation rate (R^*) increases more strontium gets incorporated in the calcite (D_{Sr} increases), and this trend is observed at all temperatures. However, the temperature seems to have no effect on the incorporation of Sr in magnesium calcite.

the Mg/Ca fluid ratio at constant rate and temperature.

The chemistry of the experiments in this work was totally different from sea water or any other natural systems. The concentration of ammonium, ammonia, chloride and other metal cations were very high comparing with natural samples. However the results of these artificial solutions in previous work as in AlKhatib and Eisenhauer (2017b) had explained the enrichment of trace metals and their isotope composition for many natural samples as ocean crust and foraminifera successfully and accurately. The precipitation rate in our work was exactly in the same range of precipitation of aragonite and calcite from sea water according to the work of Mucci et al., 1989 and close to the values of natural samples (Burton and Walter, 1987).

The calcite activation energy of precipitation from a fluid free of magnesium ions is approximately 114 kJ/mol (AlKhatib and Eisenhauer, 2017a). The presence of approximately 30 mM of Mg^{2+} ions in the

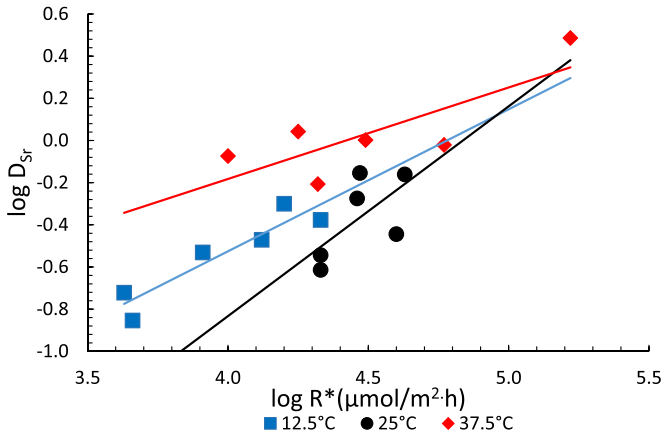

Fig. 8. log D_{Sr} in magnesium calcite overgrowths at different temperatures versus log R* (μ.mol/m^2 h). The log D_{Sr} values increase with increasing R* and independent of temperature.

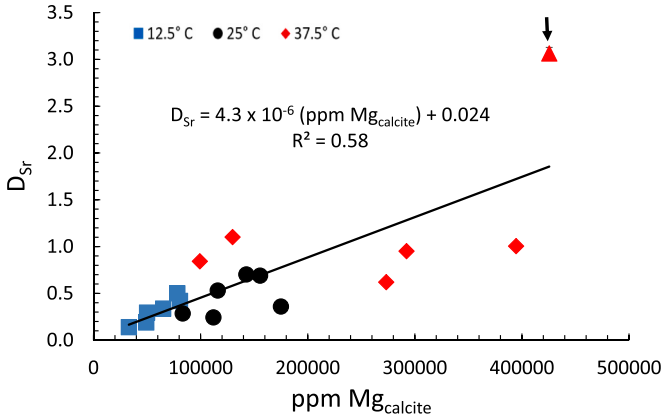

Fig. 9. D_{Sr} in magnesium calcite overgrowths as function ppm of $MgCO_3$ in calcite. As quantity of Mg increases in calcite, calcite will accommodate more Sr^{2+} ion sample reaction 16 labeled as a triangle is seem to be an anomalous value (42.55% $MgCO_3$ and D_{Sr} 3.064, Table 3) since it deviates largely from the linear correlation.

reaction fluid inhibits calcite nucleation by increasing the activation energy of calcite formation to over 149 kJ/mol (AlKhatib and Eisenhauer, 2017b). However, calcite seeds can be used to induce calcite overgrowth (e.g., Burton and Walter, 1987). The quantity of ammonium carbonate that decomposes spontaneously in the reacting chamber and the rate at which this decomposition occurs determine the concentration of DIC. As indicated in Table 1, the majority of DIC is in the form of bicarbonate ions. However, according to Andersson et al. (2016), carbonate and bicarbonate ions can be regarded as a single species because the reaction free energies for both are similar. Because the concentration of Ca^{2+} ions is almost constant (approximately 100 mM on average), the primary driving force for changing the precipitation rate is the DIC concentration. The rate of reaction is directly proportional to the DIC concentration, and the order of reaction increases with temperature (Fig. 3), which means that at constant reactant concentrations, increasing the temperature will increase the precipitation rate considerably. As the precipitation rate increases, the flux of trace elements (Mg and Sr) from the liquid to the solid will outweigh the diffusion of the trace metal ions from the solid interior toward the fluid–solid transition. As a result, more Mg and Sr will be incorporated in the calcite overgrowths as the precipitation rate increases (Figs. 7 and 8, Table 3), and HMC will be produced in most of the sample reactions. Our results are consistent with and confirm the results of Lahann and Siebert (1982) and Given and Wilkinson (1985): the enrichment of Mg in calcite is controlled by the precipitation rate. When the precipitation rate was constant, the ratio of Mg/Ca in the fluid significantly controlled the Mg enrichment in calcite at all temperatures. More Mg was incorporated in the calcite as the Mg/Ca ratio was increased from 2.9 to 3.9, as demonstrated in Table 3 for samples 1 and 6, 7 and 9, and 13 and 18 at 12.5, 25, and 37.5 °C, respectively. This result is also consistent with previous results (e.g., Mucci and Morse, 1983; De Choudens-Sánchez and González, 2009). As the temperature was increased at a constant rate, more Mg was incorporated in the calcite, as demonstrated in Fig. 7. This result is also consistent with previous results (e.g., Katz, 1973; Mucci, 1987). The progressive enrichment of Mg during extended growth retarded or completely inhibited the calcite overgrowth by pinning the steps, forming a solid solution that is more soluble than the pure phase, or by increasing the surface energy (γ) (Sun et al., 2015), As

a result, the threshold supersaturation at which overgrowths extend was gradually increased (e.g., Fernandez-Diaz et al., 1996; De Choudens-Sánchez and González, 2009), providing the opportunity for aragonite to co-precipitate with the HMC overgrowths. The mineralogy of $CaCO_3$ is significantly related to the precipitation rate (R) or DIC concentration, as indicated in Fig. 4, and it can also be related to the Mg enrichment in the calcite overgrowths.

As demonstrated in Fig. 8, as the growth rate increased, more Sr was incorporated in the calcite. This is similar to the behavior of calcite precipitated from solutions free of magnesium (AlKhatib and Eisenhauer, 2017a). However, the overgrowth calcite in this work is differentfrom the work of AlKhatib and Eisenhauer (2017a), . The D_{Sr} in this study was much higher. The increases in the D_{Sr} values and the disappearance of a clear temperature effect (the incorporation were increased in the order 25, 12.5 and 37.5C repectively)occurred due to the increasing amounts of Mg in the calcite crystal lattice (Carpenter and Lohmann, 1992). Fig. 9 illustrates a direct relationship between the D_{Sr} values and the concentration of $MgCO_3$ (Column 12 ($\times 10^4$) in Table 3) in the calcite.

$$D_{Sr} = 4.3 \times 10^{-6}\ (\text{ppm}) + 0.024 \quad (24)$$

Mucci and Morse (1983) attributed the observed Sr—Mg relationship to the distortion of the calcite crystal structure via Mg^{2+} substitution of Ca^{2+} (ionic radii = 0.72 Å and 1.00 Å, respectively). This substitution produces a localized increase in the size of the nearby cation sites and increases the incorporation of the larger Sr^{2+} ions (ionic radius 1.18 Å). Eq. (24) is in good agreement with Eq. (25) of Carpenter et al. (1991), which demonstrates the dependence of D_{Sr} on the Mg content of modern abiotic marine calcite samples.

$$D_{Sr} = 3.52 \times 10^{-6}\ (\text{ppm Mg}_{\text{calcite}}) + 0.0062 \quad (25)$$

The slight difference in the slope of Eq. (24) from that of Eq. (25) is due to the composition of our reacting solutions (containing a high concentration of NH_4^+ ions), which is different from that of seawater. The incorporation of the trace elements in sample reaction 16 (labeled as a triangle in Fig. 9) is an anomalous value (42.55% $MgCO_3$ and D_{Sr} 3.064, Table 3) because it deviates significantly from the linearity of the correlation of Eq. (24), so the credibility of this result is questionable.

5. Summary and conclusions

- The incorporation of Mg in calcite is significantly controlled by the growth rate (R*), Mg/Ca ratio of the fluid, and temperature.
- The Mg incorporated in calcite can be used as a temperature proxy of seawater if the composition of the water and the growth rate are known.
- The mineralogy of the precipitated $CaCO_3$ (precipitation of magnesium calcite or a mixture of magnesium calcite and aragonite) depends on the accumulation or the flux of dissolved inorganic carbon (DIC), as well as on the temperature.
- The D_{Sr} in calcite overgrowths depends on the precipitation rate and the quantity of $MgCO_3$ in the calcite, and it is independent of temperature. The D_{Sr} in the calcite can be used as a proxy for the precipitation rate.

Declaration of Competing Interest

The authors declare that they have no known competing financial interests or personal relationships that could have appeared to influence the work reported in this paper.

Appendix A. Appendix

Three arbitrarily selected XRD spectra (Fig. A) and their important data peaks (Table A) are presented as an example to show the difference characteristics in pure calcite and different compositions with aragonite.

The first sample number 1 is a typical pure calcite with a dominant peak spectrum at 29.4°2Θ. The second sample number 10 is (50% calcite and 50% aragonite). The third sample number 17 (20% calcite 80% aragonite). The peaks at 26.1, 27.1, 32.9 and 45.7°2Θ are the characteristic peaks for aragonite.

Table A
The count impulses at positions (°2Θ): 26.1, 27.1, 32.9, 45.7 which are finger prints of aragonite and 29.4 which is the finger print of calcite, for three arbitrary chosen samples (1, 10 and 17).

Sample	Position °2Θ	count of impulses
1	26.1	1530
1	27.1	1516
1	29.4	47,102
1	32.9	1295
1	45.7	1008
10	26.1	11,878
10	27.1	5887
10	29.4	19,057
10	32.9	5341
10	45.7	5668
17	26.1	13,172
17	27.1	6777
17	29.4	11,289
17	32.9	5444
17	45.7	6354

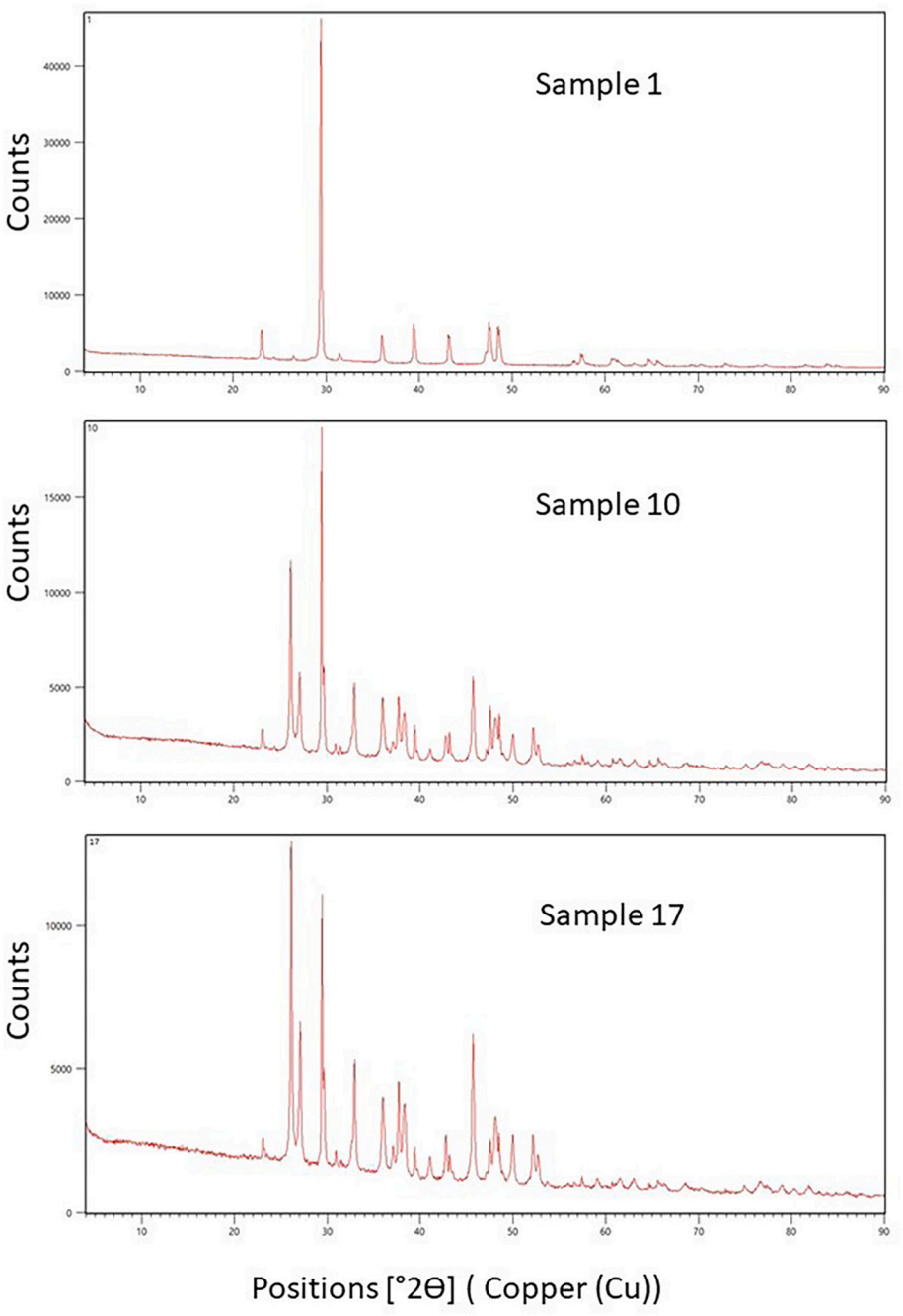

Fig. A. Three arbitrarily selected XRD spectra for samples 1 (pure calcite at 12.5 °C), sample 10 (50% calcite and 50% aragonite at 25 °C) and sample 17 (20% calcite and 80% aragonite). The dominant peak at 29.4 °2Θ is characteristic for calcite. The peaks at 26.1, 27.1, 32.9 and 45.7°2Θ are the characteristic peaks for aragonite.

References

AlKhatib, M., Eisenhauer, I., 2017a. Calcium and strontium isotope fractionation in aqueous solutions as a function of temperature and reaction rate; I. Calcite. Geochim. Cosmochim. Acta 209, 296–319.

AlKhatib, M., Eisenhauer, I.I., 2017b. Calcium and strontium isotope fractionation during precipitation from aqueous solutions as a function of temperature and reaction rate; II. Aragonite. Geochim. Cosmochim. Acta 209, 320–342.

Andersson, M.P., Rodriguez-Blanco, J.D., Stipp, S.L.S., 2016. Is bicarbonate stable in and on the calcite surface? Geochim. Cosmochim. Acta 176, 198–205.

Astilleros, J.M., Fernandez-Diaz, L., Putnis, A., 2010. The role of magnesium in the growth of calcite: an AFM study. Chem. Geol. 271, 52–58.

Bar-Matthews, M., Matthews, A., Ayalon, A., 1991. Environmental controls of speleothem mineralogy in a karstic dolomitic terrain (Soreq Cave, Israel). J. Geol. 99, 189–207.

Berner, R.A., 1975. The role of magnesium in the crystalgrowth of calcite and aragonite from seawater. Geochim. Cosmochim. Acta 39, 489–504.

Bischoff, J.L., 1968. Catalysis, inhibition, and the calcite-aragonite problem; [part] 2, the vaterite-aragonite transformation. Am. J. Sci. 266, 80–90.

Böhm, F., Eisenhauer, A., Tang, J., Dietzel, M., Krabbenhöft, A., Kisakürek, B., Horn, C., 2012. Strontium isotope fractionation of planktic foraminifera and inorganic calcite. Geochim. Cosmochim. Acta 93, 300–314.

Bryan, S.P., Marchitto, T.M., 2008. Mg/Ca-temperature proxy in benthic foraminifera: new calibrations from the Florida Straits and a hypothesis regarding Mg/Li. Paleoceanography 23, PA220.

Burton, E.A., 1993. Controls on marine carbonate cement mineralogy: review and reassessment. Chem. Geol. 105, 163–179.

Burton, E.A., Walter, L.M., 1987. Relative precipitation rates of aragonite and Mg calcite from seawater: Temperature or carbonate ion control? Geology 15, 111–114.

Burton, E., Walter, L., 1991. The effects of P_{CO2} and temperature on magnesium incorportion in calcite in seawater and $MgC1_2$-$CaC1_2$ solutions. Geochim. Cosmochim. Acta 55, 777–785.

Carpenter, S.J., Lohmann, K.C., 1992. Sr/Mg ratios in modern marine calcite: empirical indicators of ocean chemistry and precipitation rate. Geochim. et Cosmmochim. Acta 56, 1837–1849.
Carpenter, S.J., Lohmann, K.C., Holden, P., Walter, L.M., Huston, T.J., Halliday, A.N., 1991. $\delta^{18}O$ values, $^{87}Sr/^{86}Sr$ and Sr/Mg ratios of Late Devonian abiotic marine calcite: implications for the composition of ancient seawater. Geochim. Cosmochim. Acta 55, 1991–2010.
Chave, K.E., 1954a. Aspects of the biochemistry of magnesium 1. Calcareous and marine organisms. J. Geol. 62, 266–283.
Chave, K.E., 1954b. Aspects of the biochemistry of magnesium 2. Calcareous sediments and rocks. J. Geol. 62, 587–599.
Davis, K.J., Dove, P.M., De Yoreo, J.J., 2000. The role of Mg· as an impurity in calcite growth. Science 1134–1137.
De Choudens-Sánchez, V., González, L.A., 2009. Calcite and aragonite precipitation under controlled instantaneous supersaturation: elucidating the role of $CaCO_3$ saturation state and Mg/Ca ratio on calcium carbonate polymorphism. J. Sediment. Res. 79, 363–376.
De Yoreo, J.J., Vekilov, P.G., 2003. Principles of crystal nucleation and growth. In: Biomineralization. Reviews in Mineralogy & Geochemistry, 54, pp. 57–93.
Dekens, P.S., Lea, D.W., Pak, D.K., Spero, H.J., 2002. Core top calibration of Mg/Ca in tropical foraminifera: refining paleotemperature estimation. Geochem. Geophys. Geosyst. 3 (4), 1–29.
Dickson, J.A.D., 2002. Fossil echinoderms as monitor of the Mg/ca ratio of Phanerozoic oceans. Science 298, 1222–1224.
Elderfield, H., Ganssen, G., 2000. Past temperature and 5180 of surface ocean waters inferred from foraminiferal Mg/Ca ratios. Nature 405, 442–445.
Elderfield, H., Bertram, C.J., Erez, J., 1996. A biomineralization model for the incorporation of trace elements into foraminiferal calcium carbonate. Earth Planet. Sci. Lett. 142, 409–423.
Falini, G., Gazzano, M., Ripamonti, A., 1994. Crystallization of calcium carbonate in presence of magnesium and polyelectrolytes. J. Cryst. Growth 137, 577–584.
Fernandez-Diaz, L., Putnis, A., Prieto, M., Putnis, C.V., 1996. The role of magnesium in the crystallization of calcite and aragonite in a porous medium. J. Sediment. Res. 66 (3), 482–491.
Folk, R.L., 1974. The natural history of crystalline calcium carbonate: effect of magnesium content and salinity. J. Sediment. Petrol. 44, 40–53.
Given, R.K., Wilkinson, B.H., 1985. Kinetic control of morphology, composition, and mineralogy of abiotic sedimentary carbonates. J. Sediment. Petrol. 55, 109–119.
Hartley, G., Mucci, A., 1996. The influence of P_{CO2} on the partitioning of magnesium in calcite overgrowths precipitated from artificial seawater at 25″ and 1 atm total pressure. Geochim. Cosmochim. Acta 60 (2), 315–324.
Hathorne Ed, C., Gagnon, A., Felis, T., et al., 2013. Interlaboratory study for coral Sr/Ca and other element/Ca ratio measurements. G3 Geochem. Geophys. Geosyst. 14 (9), 3730–3750.
Howson, M.R., Pethybridge, A.D., House, W.A., 1987. Synthesis and distribution coefficient of low-magnesium calcites. Chem. Geol. 64, 79–87.
Katz, A., 1973. The interaction of magnesium with calcite during crystal growth at 25-90°C and one atmosphere. Geochim. Cosmochim. Acta 37, 1663–1586.
Kubota, N., Mullin, J.W., 1995. A kinetic model for crystal growth from aqueous solution in the presence of impurity. J. Cryst. Growth 152, 203–208.
Lahann, R.W., Siebert, R.M., 1982. A kinetic model for distribution coefficients and application to Mg-calcites. Geochim. et Cosmo 46 (11), 2229–2237.
Lea, D.W., Mashiotta, T.A., Spero, H.J., 1999. Controls on magnesium and strontium uptake in planktonic foraminifera determined by live culturing. Geochim. Cosmochim. Acta 63, 2369–2379.
Lemarchand, D., Wasserburg, G.J., Papanastassiou, D.A., 2004. Rate-controlled calcium isotope fractionation in synthetic calcite. Geochim. Cosmochim. Acta 68, 4665–4678.
Lopez, O., Zuddas, P., Faivre, D., 2009. The influence of temperature and seawater composition on calcite crystal growth mechanisms and kinetics: implications for Mg incorporation in calcite lattice. Geochim. Cosmochim. Acta 73, 337–347.
Meldrum, F.C., Hyde, S.T., 2001. Morphological influence of magnesium and organic additives on the precipitation of calcite. J. Cryst. Growth 231, 544–558.
Millero, F.J., 1995. Thermodynamics of the carbon dioxide system in the oceans. Geochim. Cosmochim. Acta 59, 661–677.
Morse, J.W., 1983. The kinetics of calcium carbonate dissolution and precipitation. In: Reeder, R.J. (Ed.), Carbonates: Mineralogy and Chemistry, Mineralogical Society of America, Reviews in Mineralogy, pp. 227–264.
Morse, J.W., Bender, M.L., 1990. Partition coefficients in calcite: examination of factors influencing the validity of experimental results and their application to natural systems. Chem. Geol. 82, 265–277.
Morse, J.W., He, S., 1993. Influences of T, S and PCO_2 on the pseudohomogeneous nucleation of calcium carbonate from seawater: implications for whiting formation. Mar. Chem. 41, 291–298.
Morse, J.W., Mackenzie, F.T., 1990. Geochemistry of Sedimentary Carbonates. Elsevier, Amsterdam.
Morse, J.W., Wang, Q., Tsio, M.Y., 1997. Influences of temperature and Mg:Ca ratio on CaCO3 precipitates from seawater. Geology 25, 85–87.
Mucci, A., 1986. Growth kinetics and composition of magnesian calcite overgrowths precipitated from seawater: quantitative influence of orthophosphate ions. Geochim. Cosmochim. Acta 50, 2255–2265.
Mucci, A., 1987. Influence of temperature on the composition of magnesian calcite overgrowths precipitated from seawater. Geochim. Cosmochim. Acta 51, 1977–1984.
Mucci, A., Morse, J.W., 1983. The incorporation of Mg^{2+} and Sr^{2+} into calcite overgrowths: influence of growth rate and solution composition. Geochim. Cosmochim. Acta 47, 217–233.
Mucci, A., Canuel, R., Zhong, S., 1989. The solubility of calcite and aragonite in sulfate-free seawater and the seeded growth kinetics and composition of the precipitates at 25 ° C. Chem. Geol. 74, 309–320.
Niedermayr, A., Köhler, S.J., Dietzel, M., 2013. Impacts of aqueous carbonate accumulation rate, magnesium and polyaspartic acid on calcium carbonate formation (6–40 °C). Chem. Geol. 340, 105–120.
Plummer, L.N., Busenberg, E., 1982. The solubilities of calcite, aragonite and vaterite in CO_2–H_2O solutions between 0 and 90 °C, and an evaluation of the aqueous model for the system $CaCO_3$–CO_2–H_2O. Geochim. Cosmochim. Acta 46, 1011–1040.
Rosenthal, Y., Boyle, E.A., Slowey, N., 1997. Temperature control on the incorporation of magnesium, strontium, fluorine, and cadmium into benthic foraminiferal shells from Little Bahama Bank: prospects for thermoc1ine paleoceanography. Geochim. Cosmochim. Acta 61, 3633–3643.
Scoffin, T.P., 1987. An Introduction to Carbonate Sediments and Rocks. Chapman & Hall, New York, p. 274.
Stanley, S.M., 1999. Earth System History. W. H, Freeman, New York, p. 615. Stanley S. M.
Stanley, S.M., Hardie, L.A., 1998. Secular oscillations in the carbonate mineralogy of reefbuilding and sediment-producing organisms driven by tectonically forced shifts in seawater chemistry. Palaeogeogr. Palaeoclimatol. Palaeoecol. 144, 3–19.
Sun, W., Jayaraman, S., Chen, W., Persson, K.A., Ceder, G., 2015. Nucleation of metastable aragonite $CaCO_3$ in seawater. Appl. Phys. Sci. 112 (11), 3199–3204.
Tang, J., Niedermayr, A., Köhler, S.J., Böhm, F., Kisakürek, B., Eisenhauer, A., Dietzel, M., 2012. Sr2+/Ca2+ and 44Ca/40Ca fractionation during inorganic calcite formation: III. Impact of salinity/ionic strength. Geochim. Cosmochim. Acta 77, 432–443.
Urey, H.C., Lowenstam, H.A., Epstein, S., McKinney, C.R., 1951. Measurements of paleotemperatures and temperatures of the Upper Cretaceous of England, Denmark, and the southeastern United States. Geol. Soc. Am. Bull. 62, 399.
Usdowski, H.E., 1975. Fraktionierung der Spurenelemente bei der Kristallisation. Springer-Verlag, Berlin, Heidelberg, 104 pp.
van Enckevort, W.J.P., van den Berg, A.C.J.F., Kreuwel, K.B.G., Derksen, A.J., Couto, M. S., 1996. Impurity blocking of growth steps: experiments and theory. J. Cryst. Growth 166, 156–161.
Weber, J.N., Woodhead, P.M., 1970. Carbon and oxygen isotope fractionation in skeletal carbonate of reef-building corals. Chem. Geol. 6, 93–117.
Weber, J.N., Woodhead, P.M., 1972. Temperature dependence of oxygen-18 concentration in reef coral carbonates. J. Geophys. Res. 77, 463–473.
Zhong, S., Mucci, A., 1989. Calcite and aragonite precipitation from seawater solutions of various salinities: Precipitation rates and overgrowth compositions. In: Schott, J., Lasaga, A.C. (Eds.), Kinetic Geochemistry.Chem. Geol, 78, pp. 283–299.